Electronic Supplementary Material (ESI) for Lab on a Chip.
This journal is © The Royal Society of Chemistry 2024

Supporting Information

Ultra-Low Intensity Light Pulses for Large Cargo Delivery into Hard-to-Transfect Cells using rGO Mixed PDMS Microtip Device

Hima Harshan Padma [a], Kavitha Illath [a], Donia Dominic [a], Hwan-You Chang [b], Moeto Nagai [c], Rajdeep Ojha [d], Srabani Kar [e], Tuhin Subhra Santra [a*]

[a] Department of Engineering Design, Indian Institute of Technology Madras, India

[b] Department of Medical Science, National Tsing Hua University, Taiwan

[c] Department of Mechanical Engineering, Toyohashi University of Technology

[d] Department of Physical Medicine and Rehabilitation, Christian Medical College, Vellore, India

[e] Department of Physics, Indian Institute of Science Education and Research Tirupati, India

*tuhin@iitm.ac.in & santra.tuhin@gmail.com

Table S1: The summary of notable works on NPs-mediated photoporation

NPs Material	Laser Wavelength (nm)	Laser energy/ Fluence	Exposure time	Molecules	Cells	No: of cell/Cell volume	Efficiency (%)	Viability (%)	Ref.
Cationic PDDAC-coated gold	561	0.9 J cm−2	~ 3 min	eGFP-mRNA delivery	Jurkat T cells	-	24	14	1
Gold	532	1.60 J/cm^2	3 min	Cas9 ribonucleoprotein (RNP) complexes	lung epithelial cell line-H1299	-	96	80	2
Carbon-black	1064	25-29 mJ/cm^2	4-5 min	Dextran 4kDa Dextran 2000 kDa	DU145 prostate cancer	-	43 18	55 25	3
Gold NPs layer	808	1 W cm $^{-2}$	300 s	Dextran	mouse embryonic fibroblasts (mEFs)	-	53 & 19	80 & 88	4
				plasmid DNA	human umbilical vein endothelial cells (HUVECs	-	44 & 8	90 & 87	

Gold	561	0.96 J/cm^2	7s	Dextran 10 kDa	primary human CD4+ T cells	-	62	32	[5]
rGO-PEG	800	0.89 J/cm^2	2.1 mm/s (scanning speed)	Dextran 10 kDa	HeLa	-	80	80	[6]
rGO mixed PDMS microtip device	900	0.9J/cm^2	5s	PI Dextran Enzyme	SiHa	80,000 ± 20,000	**96** **97** **95**	**97** **97** **98**	Present work

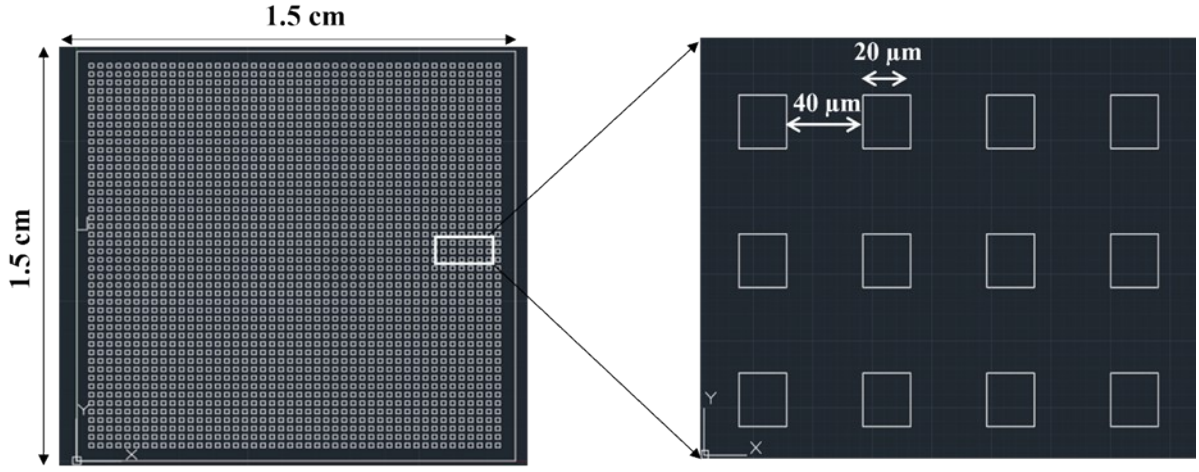

Fig S1: AutoCAD design of square pattern for microtip device with overall dimension of 1.5 × 1.5 cm^2. 20 × 20 µm^2 individual square dimension and 40 µm of edge-to-edge distance between the adjacent squares.

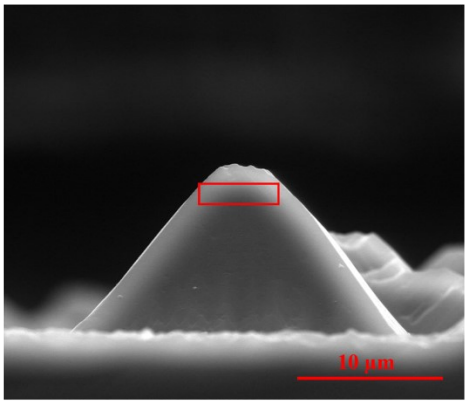

Element	Wt%	At%
CK	56.46	69.88
OK	21.15	19.94
SiK	26.39	14.17
Matrix	Correction	ZAF

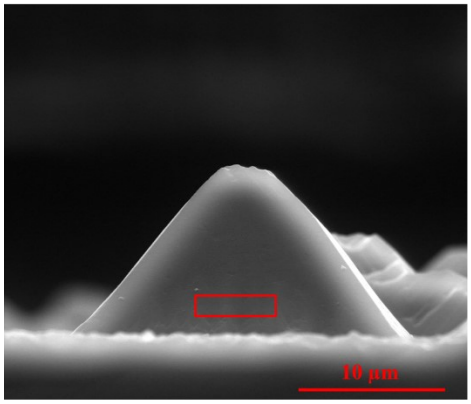

Element	Wt%	At%
CK	37.19	47.09
OK	20.32	24.99
SiK	36.49	21.36
Matrix	Correction	ZAF

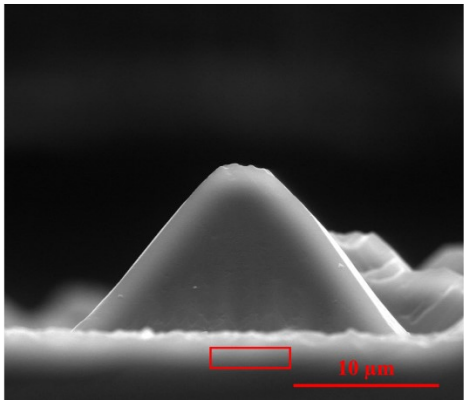

Element	Wt%	At%
CK	33.11	44.75
OK	21.09	28.54
SiK	37.98	26.71
Matrix	Correction	ZAF

Fig S2: SEM-EDAX characterisation of rGO mixed pyramidal microtip device. SEM images (left column) and elemental distribution results (right column) of red squared area in the corresponding image. The scale bar shown here cannot be correlate with the device dimension, because of the distance and angle in capturing the image.

Table S2: Summary of parameters used in the COMSOL simulation of rGO mixed PDMS microtip device

Parameter	**Value**	**Ref.**
C_l	0.7 J (kg K) $^{-1}$	7
Density of rGO, ρ_r	2267 kg/m^3	8
RGO electron-acoustic phonon cooling rate, Γ^{e-ph}	C_P /2 ps, 2ps is taken to be average heat transfer rate from carrier to acoustic phonon	9
Graphene/water heat transfer coefficient	30 $MW\ m^{-2}K^{-1}$	10,11
Graphene/PDMS heat transfer coefficient	3 W $m^{-2}K^{-1}$	12
Water density, ρ_w	997 kg/m^3	
PDMS density, ρ_w	970 kg/m^3	
Graphene electronic thermal conductivity	2500 W (m K) $^{-1}$	7
Graphene lattice thermal conductivity	2000 W (m K) $^{-1}$	13

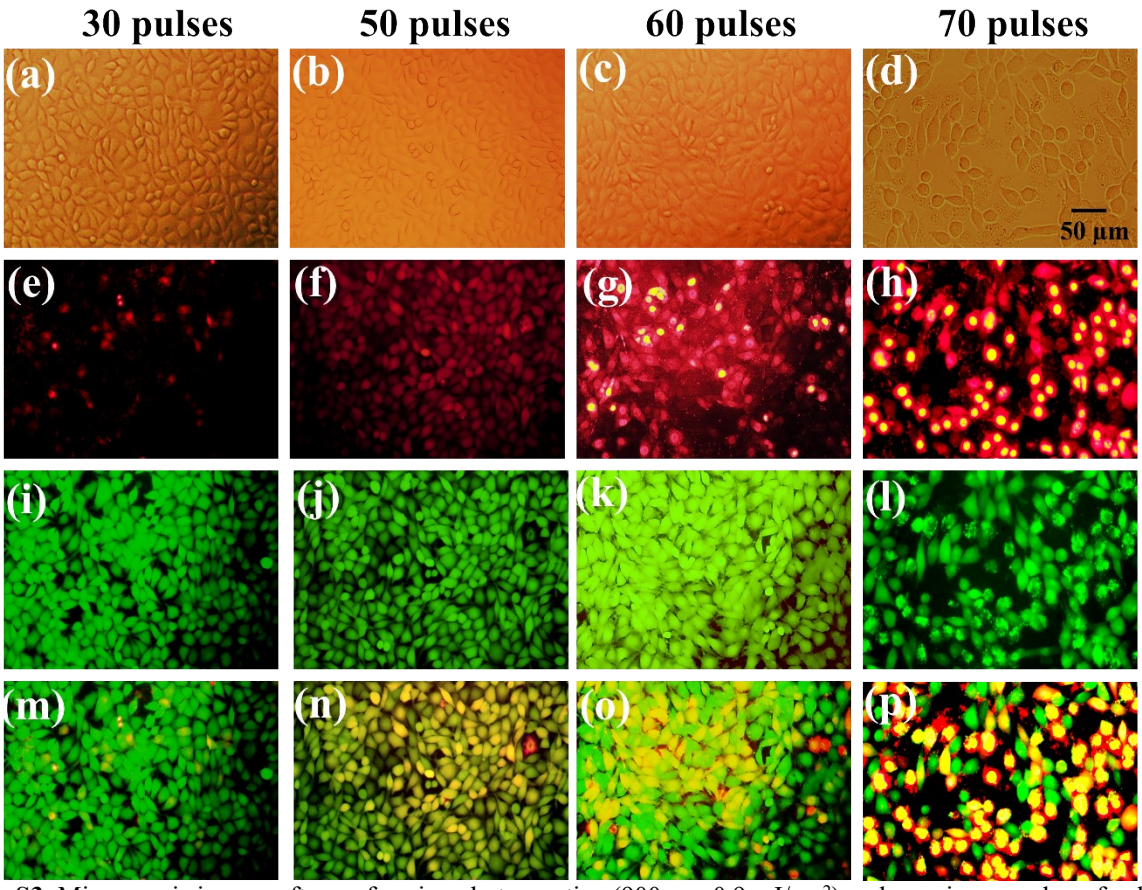

Fig S3: Microscopic images after performing photoporation (900 nm, 0.9 mJ/cm^2) under various number of pulses in delivering PI into L929 cells.

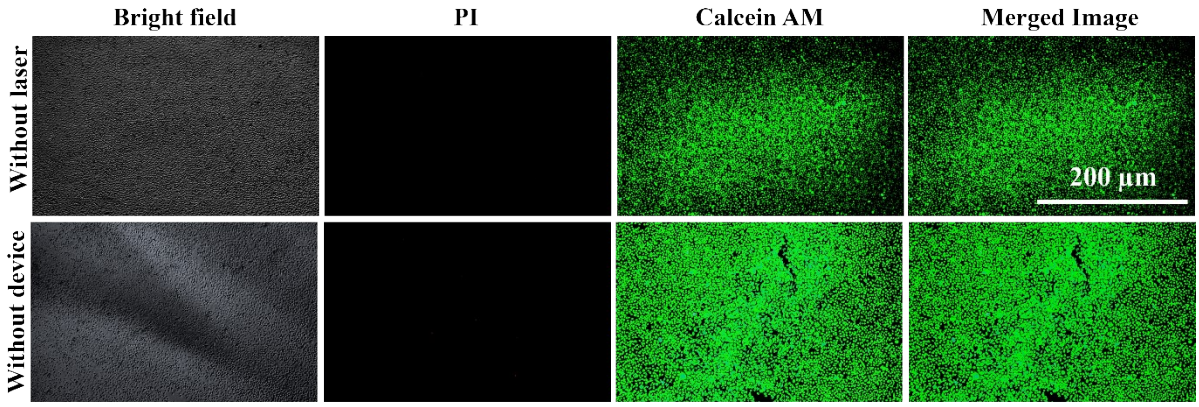

Fig S4: PI delivery in controls. Images captured after performing photoporation without rGO mixed PDMS pyramidal microtip device (top row) and with device in the absence of laser

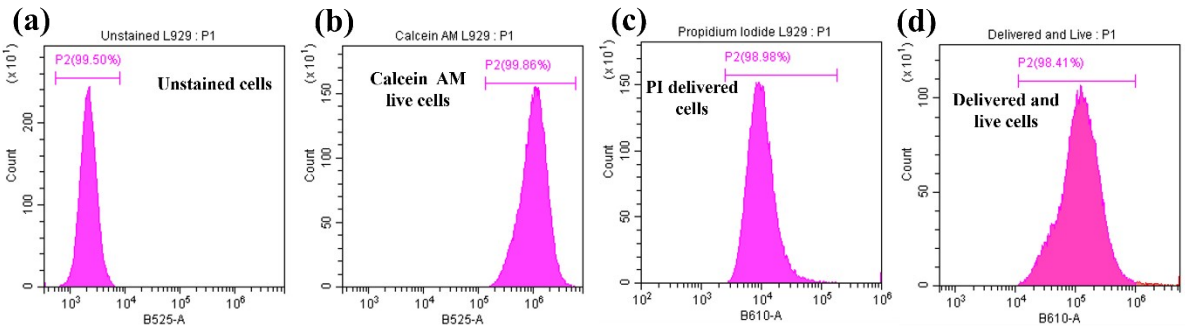

Fig S5: Flow cytometry-based histogram in L929 showing **(a)** unstained cells, **(b)** calcein AM stained live cells, **(c)** PI delivered cells, and **(d)** dual stained PI delivered and live cells.

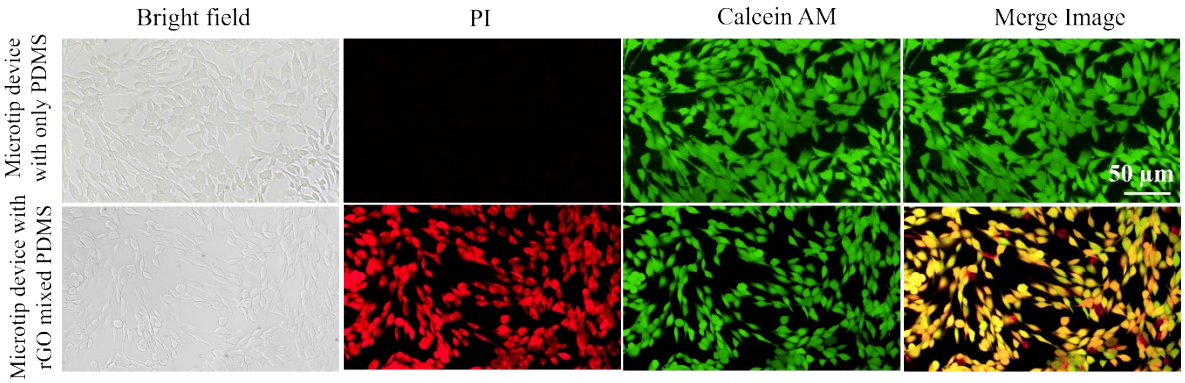

Fig S6: Photoporation results after with PDMS and with rGO mixed PDMS Microtip device. Images captured after performing photoporation with PDMS Microtip device (top row) and with rGO mixed PDMS pyramidal microtip device

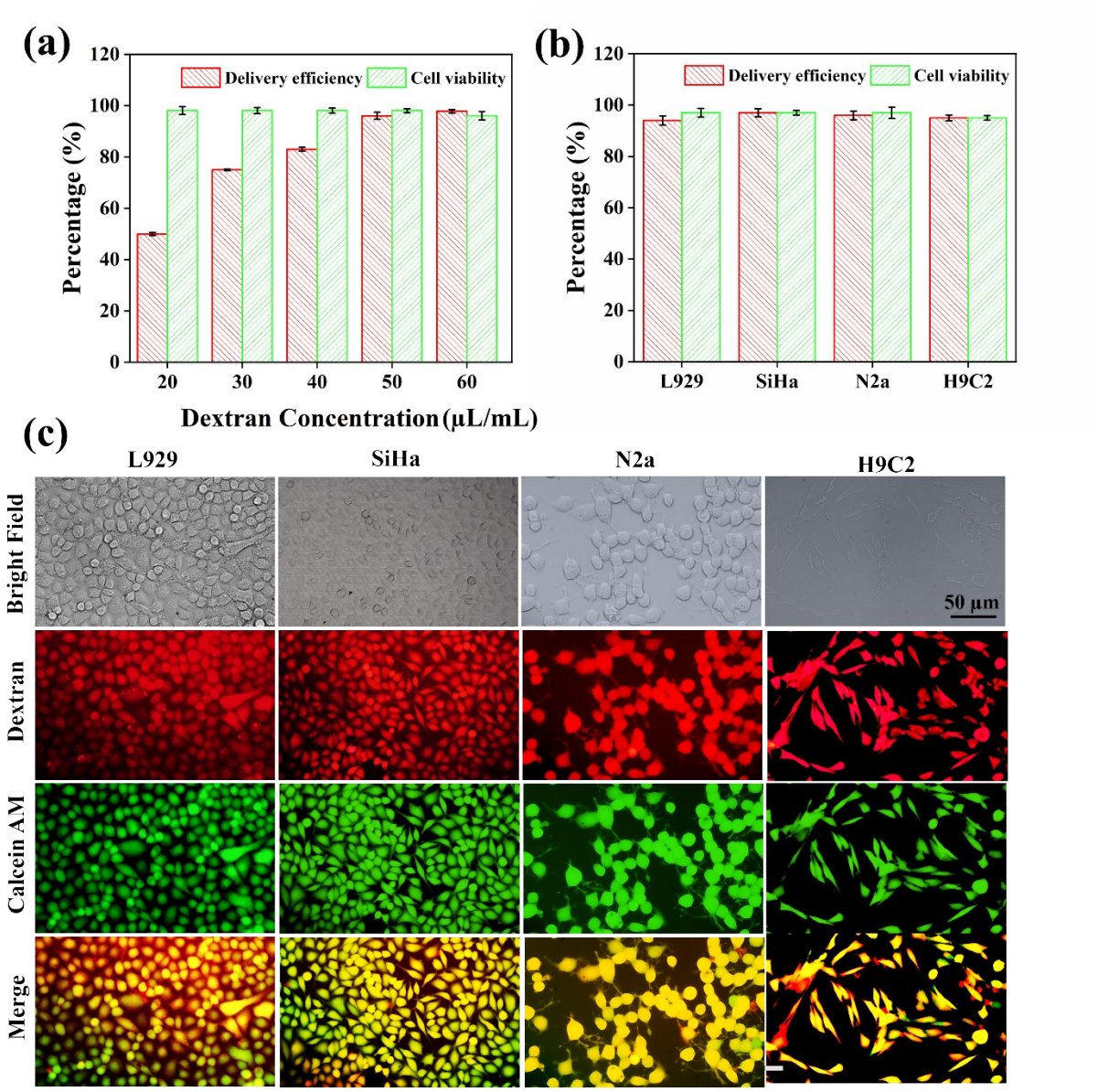

Fig S7: Delivery of Dextran 3000 Da. (a) assessment of delivery efficiency and cell viability with different dextran concentrations into L929 cells at a laser energy of 0.25 mJ for 50 pulses, **(b)** quantification of delivery efficiency and cell viability after dextran delivery into L929, SiHa, N2a and H9C2 cells (n = 3 independent experiments, data presented as mean ± S.D.), **(c)** microscopic images of cells after dextran (3000 Da) delivery using the rGO-PDMS microtip device assisted photoporation into L929, SiHa, N2a, H9C2 cells.

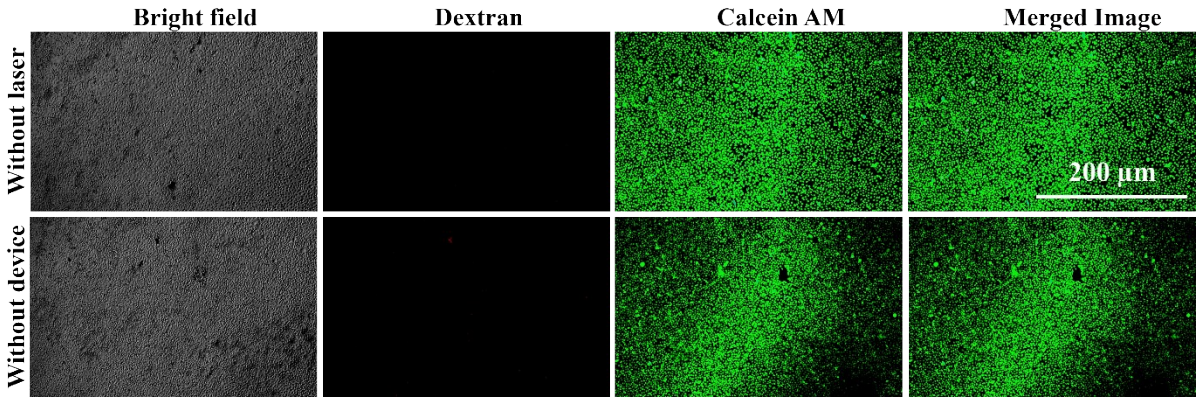

Fig S8: Dextran delivery in controls. Images captured after performing photoporation without rGO mixed PDMS pyramidal microtip device (top row) and with device in the absence of laser.

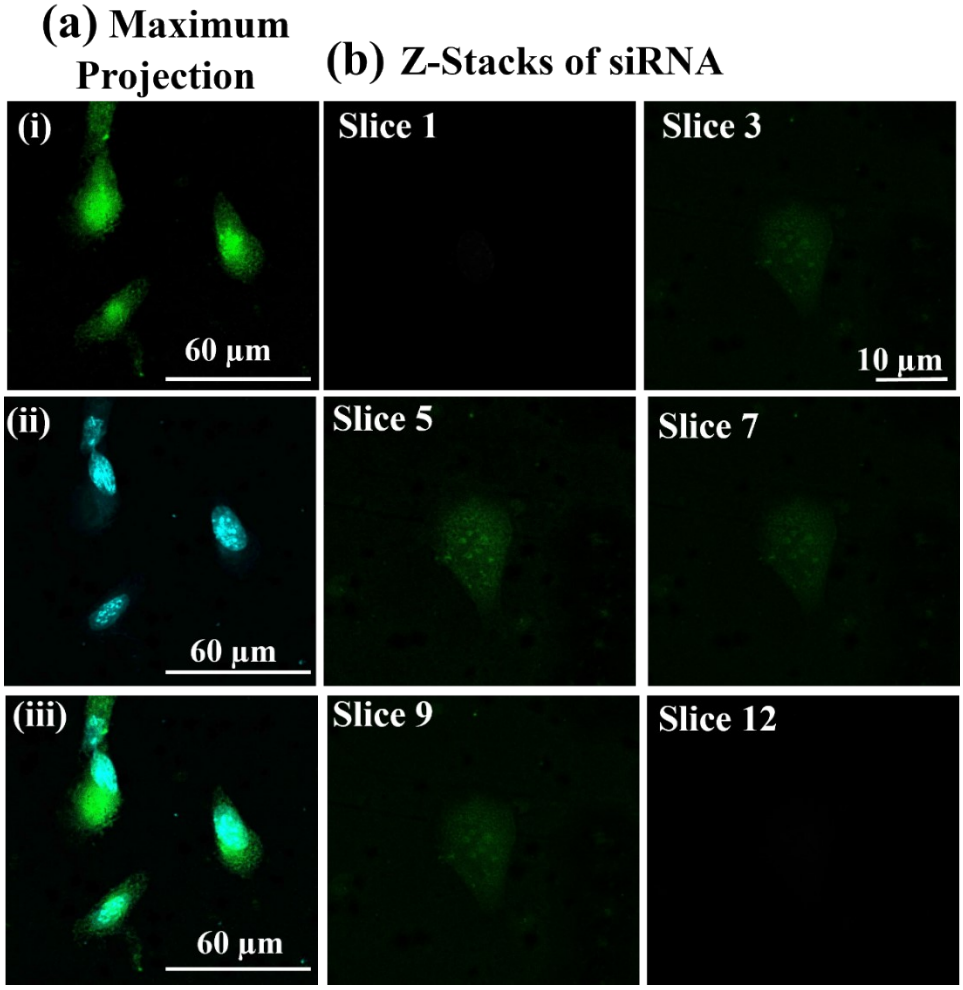

Fig S9: Confocal scanning images of 3T3 cells after siRNA delivery **(a)** maximum projection (i) siRNA delivery, (ii) nucleus staining due to Hoechst 33342 and (iii) merged image and **(b)** 12 slices which are equally divided and confirms the successful delivery using rGO mixed PDMS microtips device based photoporation.

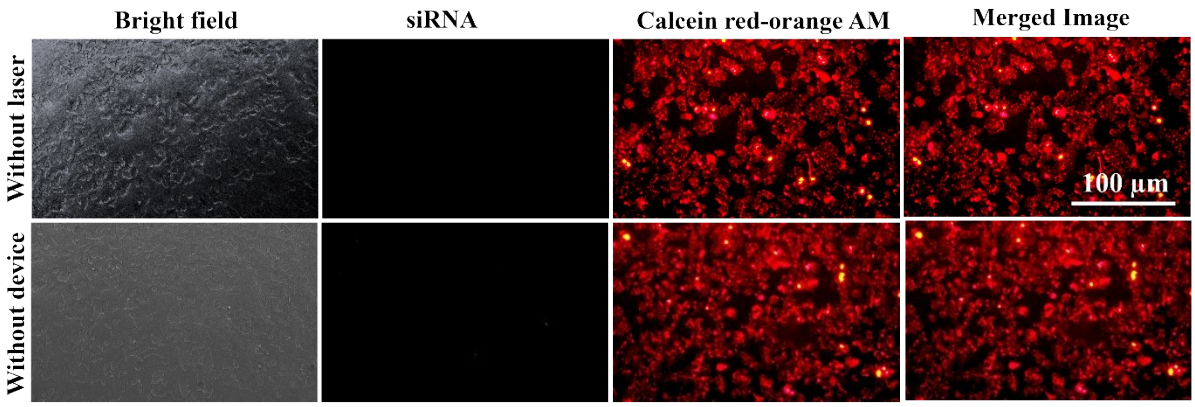

Fig S10: siRNA delivery in controls. Images captured after performing photoporation without rGO mixed PDMS pyramidal microtip device (top row) and with device in the absence of laser.

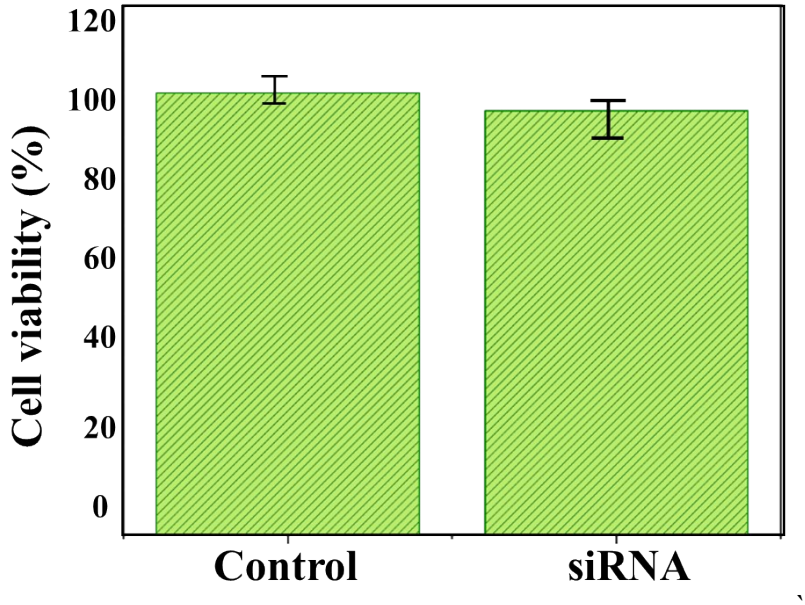

Fig S11: Cell viability results in L929 cells using MTT assay 24 hrs. after laser exposure with wavelength at 900 nm, fluence of 0.9 mJ/cm^2, and 50 pulses for siRNA delivery using rGO mixed PDMS microtip device.

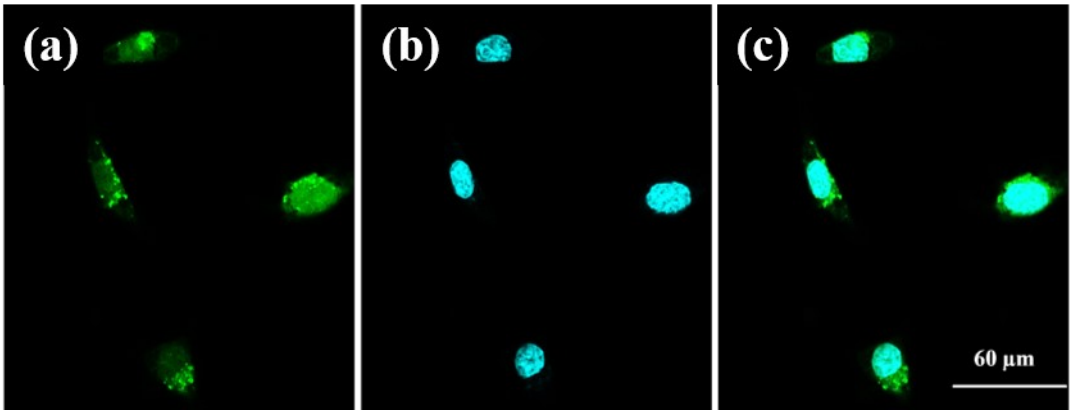

Fig S12: (a, b,c) Confocal images of L929 cells after performing photoporation (900 nm, 0.9 mJ/cm2, 50 pulses) revealing EGFP delivery, nucleus staining using Hoechst 33342 dye and merged image, respectively.

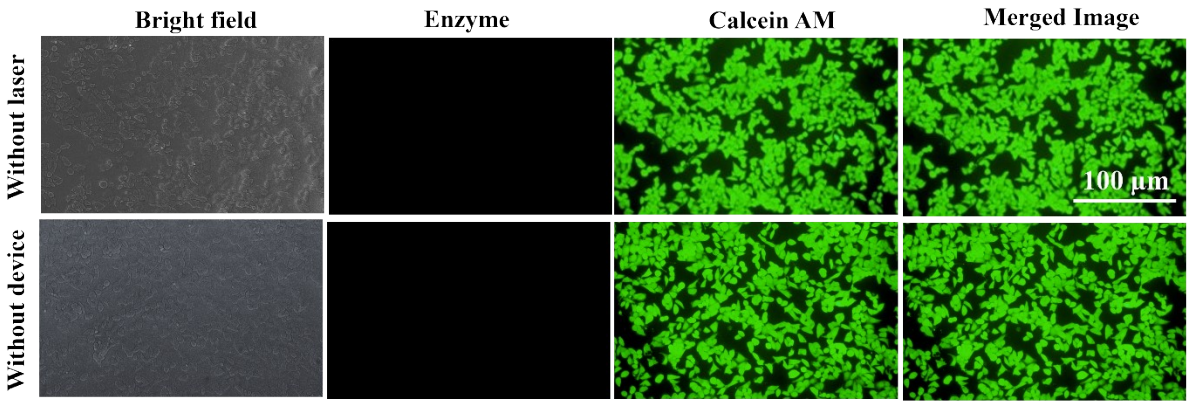

Fig S13: Enzyme delivery in controls. Images captured after performing photoporation without rGO mixed PDMS pyramidal microtip device (top row) and with device in the absence of laser.

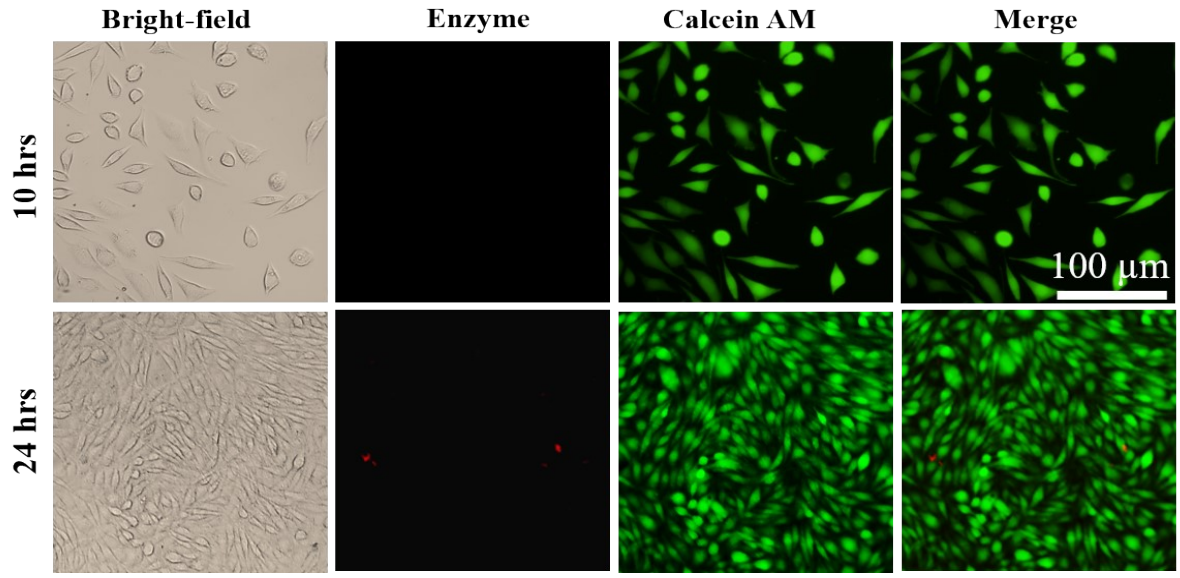

Fig S14: Control experiments to check endocytosis or micropinocytosis induced delivery: Microscopic images captured after incubating cells with enzymes for 10 hrs and 24 hrs.

Table S3: Comparison of our delivery platform with existing intracellular delivery platform

Parameters	**Mechanoporation** [14]	**Photoporation** [15]	**Photoporation using rGO mixed Microtip device (present work)**
Technique used	Lithography	Lithography	Lithography
Intracellular Delivery Method	Puncture loading	Nanosecond pulse laser	Nanosecond Pulse laser

Nanostructures materials	Silicon nanoneedles	Silicon microneedles	rGO
Wavelength	--		Infrared (900 nm)
Biomolecules Delivered	Dextran 70/500, Calcein	Dextran 10/70/150/500/2000, Calcein	PI, Dextran, EGFP plasmid, Cas9 plasmid, Enzyme
Delivery Efficiency	Calcein – **50%** Dextran 500 - **20%**	Dextran 10- **80%** Dextran 2000- **18%**	PI - SiHa: **96%,** Dextran – SiHa: **97%** Enzyme (465 kDa) - SiHa: **95%**
Cell Viability	Calcein- **80%** Dextran 500 – **95%**	Dextran 10- **97%** Dextran 2000- **94%**	PI - SiHa: **97%** Dextran – SiHa: **97%** Enzyme - SiHa: **98%**

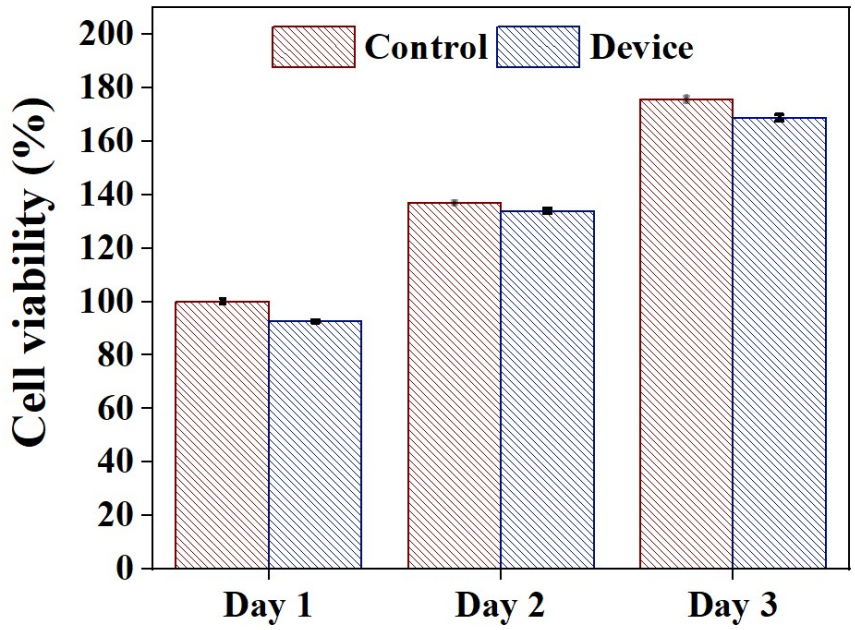

Fig S15: Cell viability results in L929 cells using MTT assay for three days after laser exposure with wavelength at 900 nm, fluence of 0.9 mJ/cm^2, and 50 pulses in rGO mixed PDMS microtip device.

References

1 L. Raes, S. Stremersch, J. C. Fraire, T. Brans, G. Goetgeluk, S. De Munter, L. Van Hoecke, R. Verbeke, J. Van Hoeck, R. Xiong, X. Saelens, B. Vandekerckhove, S. De Smedt, K. Raemdonck and K. Braeckmans, *Nano-Micro Lett.*, 2020, **12**, 1–17.

2 L. Raes, M. Pille, A. Harizaj, G. Goetgeluk, J. Van Hoeck, S. Stremersch, J. C. Fraire, T. Brans, O. G. de Jong, R. Maas-Bakker, E. Mastrobattista, P. Vader, S. C. De Smedt, B. Vandekerckhove, K. Raemdonck and K. Braeckmans, *Mol. Ther. - Nucleic Acids*, 2021, **25**, 696–707.

3 S. Kumar, A. Li, N. N. Thadhani and M. R. Prausnitz, *Nanomedicine Nanotechnology, Biol. Med.*, 2021, **37**, 102431.

4 Z. Lyu, F. Zhou, Q. Liu, H. Xue, Q. Yu and H. Chen, *Adv. Funct. Mater.*, 2016, **26**, 5787–5795.

5 L. Raes, C. Van Hecke, J. Michiels, S. Stremersch, J. C. Fraire, T. Brans, R. Xiong, S. De Smedt, L. Vandekerckhove, K. Raemdonck and K. Braeckmans, *Crystals*, 2019, **9**, 411.

6 J. Liu, C. Li, T. Brans, A. Harizaj, S. Van de Steene, T. De Beer, S. De Smedt, S. Szunerits, R. Boukherroub, R. Xiong and K. Braeckmans, *Int. J. Mol. Sci.*, 2020, **21**, 1540.

7 Q.-Y. Li, K. Xia, J. Zhang, Y. Zhang, Q. Li, K. Takahashi and X. Zhang, *Nanoscale*, 2017, **9**, 10784–10793.

8 L. Torrisi, M. Cutroneo, A. Torrisi and L. Silipigni, *Phys. status solidi*, 2022, **219**, 1–9.

9 C. H. Lui, K. F. Mak, J. Shan and T. F. Heinz, *Phys. Rev. Lett.*, 2010, **105**, 127404.

10 Y. Ma, Z. Zhang, J. Chen, K. Sääskilahti, S. Volz and J. Chen, *Carbon N. Y.*, 2018, **135**, 263–269.

11 S. Chen, M. Yang, B. Liu, M. Xu, T. Zhang, B. Zhuang, D. Ding, X. Huai and H. Zhang, *RSC Adv.*, 2019, **9**, 4563–4570.

12 Y. Liu, M. Lu, K. Wu, E. Jiao, L. Liang, J. Shi and M. Lu, *Compos. Sci. Technol.*, 2021, **213**, 108940.

13 E. Pop, V. Varshney and A. K. Roy, *MRS Bull.*, 2012, **37**, 1273–1281.

14 S. Park, S.-O. Choi, S. Paik, S. Choi, M. Allen and M. Prausnitz, *Biomed. Microdevices*, 2016, **18**, 10.

15 N. Saklayen, S. Kalies, M. Madrid, V. Nuzzo, M. Huber, W. Shen, J. Sinanan-Singh, D. Heinemann, A. Heisterkamp and E. Mazur, *Biomed. Opt. Express*, 2017, **8**, 4756.